Supplemental Material for Realizing Fractional Chern Insulators with Dipolar Spins

I. DERIVATION OF THE EFFECTIVE HAMILTONIAN

Here, we derive the effective Hamiltonian, $H_B = -\sum_{ij} t_{ij} a_i^\dagger a_j + \frac{1}{2}\sum_{i\neq j} V_{ij} n_i n_j$ (Eqn. 3 of the main text). The geometry is shown in the inset of Fig. 1A. The molecules lie in the X-Y plane and are governed by a Hamiltonian $H_m = BJ^2 - d^z E$, where E is the applied electric field, which has spherical coordinates (Θ_0, Φ_0) in the $\{X, Y, Z\}$ basis. To simplify the notation, we define $|\uparrow\rangle = s|1,-1\rangle + v|1,1\rangle + w|1,0\rangle$, where $s = \Omega_2\Omega_4/\tilde{\Omega}$, $v = \Omega_1\Omega_3/\tilde{\Omega}$, $w = -\Omega_1\Omega_4/\tilde{\Omega}$. Consider two dressed molecules at positions i and j separated by $\mathbf{R} = (R, \theta, \phi)$ (spherical coordinates in the $\{x, y, z\}$ basis). The dipolar interaction between these molecules can be written in spherical tensor form as:

$$H_{\rm dd} \;=\; -\frac{1}{4\pi\epsilon_0}\frac{\sqrt{6}}{R^3}\sum_{q=-2}^{2}(-1)^q C^2_{-q}(\theta,\phi) T^2_q(\mathbf{d}_i, \mathbf{d}_j), \tag{S1}$$

where $C^k_q(\theta,\phi)$ is the spherical harmonic of degree k and z angular momentum q with the normalization of [26]. Here, T^2 is the rank 2 spherical tensor generated from the dipole operators; in particular, $T^2_{\pm 2}(\mathbf{d}_i, \mathbf{d}_j) = d_i^\pm d_j^\pm$, $T^2_{\pm 1}(\mathbf{d}_i, \mathbf{d}_j) = \left(d_i^z d_j^\pm + d_i^\pm d_j^z\right)/\sqrt{2}$, $T^2_0(\mathbf{d}_i, \mathbf{d}_j) = \left(d_i^- d_j^+ + 2d_i^z d_j^z + d_i^+ d_j^-\right)/\sqrt{6}$, and $d^\pm = \mp(d^x \pm i d^y)/\sqrt{2}$. Expressing the dipolar interaction in this form allows us to isolate energy conserving terms. We assume that the energy difference between $|1,0\rangle$ and $|1,\pm 1\rangle$ (Δ in Fig. 1B) is larger than the scale of the dipole-dipole interactions. Under this assumption, $T^2_{\pm 1}$ terms of the dipolar interaction are energy non-conserving and thus highly suppressed.

We now consider the three resonant contributions to the hopping (t_{ij}) matrix elements,

$$\langle\uparrow_i\downarrow_j| T^2_0 |\downarrow_i\uparrow_j\rangle \;=\; \sqrt{\frac{2}{3}}[d^2_{00} w_i^* w_j - \frac{1}{2} d^2_{01}(v_i^* v_j + s_i^* s_j)], \tag{S2}$$

$$\langle\uparrow_i\downarrow_j| T^2_{+2} |\downarrow_i\uparrow_j\rangle \;=\; -d^2_{01}(v_i^* s_j), \tag{S3}$$

$$\langle\uparrow_i\downarrow_j| T^2_{-2} |\downarrow_i\uparrow_j\rangle \;=\; -d^2_{01}(s_i^* v_j), \tag{S4}$$

where $d_{00} = \langle 1,0|d^z|0,0\rangle$ and $d_{01} = \langle 1,\pm 1|d^\pm|0,0\rangle$. Combined with the spherical harmonic coefficients of Eqn. (S1), these terms determine the directionally dependent hopping t_{ij} of the spin flips.

The interactions V_{ij} between the spin flips arise as a consequence of the induced dipole moment which each molecule acquires in an applied electric field. Thus, $V_{ij} = \langle\uparrow_i\uparrow_j| H_{dd} |\uparrow_i\uparrow_j\rangle + \langle\downarrow_i\downarrow_j| H_{dd} |\downarrow_i\downarrow_j\rangle - \langle\uparrow_i\downarrow_j| H_{dd} |\uparrow_i\downarrow_j\rangle - \langle\downarrow_i\uparrow_j| H_{dd} |\downarrow_i\uparrow_j\rangle$ can be calculated in a similar fashion. First, let us define the induced dipole moment of a molecule on site i, $d_{\uparrow_i} = d_1(|s_i|^2 + |v_i|^2) + \mu_0|w_i|^2$, where $d_1 = \langle 1,\pm 1|d^z|1,\pm 1\rangle$ and $\mu_0 = \langle 1,0|d_z|1,0\rangle$ that of the $|1,0\rangle$ state. The contributing terms to V_{ij} are then (suppressing ij subscripts in $\mathbf{d}$):

$$\langle\downarrow_i\downarrow_j| d^z d^z + \frac{1}{2}(d^+ d^- + d^- d^+) |\downarrow_i\downarrow_j\rangle \;=\; d_0^2, \tag{S5}$$

$$\langle\uparrow_i\downarrow_j| d^z d^z + \frac{1}{2}(d^+ d^- + d^- d^+) |\uparrow_i\downarrow_j\rangle \;=\; d_{\uparrow_i} d_0, \tag{S6}$$

$$\langle\downarrow_i\uparrow_j| d^z d^z + \frac{1}{2}(d^+ d^- + d^- d^+) |\downarrow_i\uparrow_j\rangle \;=\; d_0 d_{\uparrow_j}, \tag{S7}$$

$$\langle\uparrow_i\uparrow_j| d^z d^z + \frac{1}{2}(d^+ d^- + d^- d^+) |\uparrow_i\uparrow_j\rangle \;=\; d_{\uparrow_i} d_{\uparrow_j} - \frac{1}{2}\mu^2_{01}(s_i w_i^* w_j s_j^* + w_i v_i^* v_j w_j^* + \text{c.c.}), \tag{S8}$$

$$\langle\uparrow_i\uparrow_j| d^+ d^+ |\uparrow_i\uparrow_j\rangle \;=\; -\mu^2_{01}(s_i w_i^* w_j v_j^* + w_i v_i^* s_j w_j^*), \tag{S9}$$

$$\langle\uparrow_i\uparrow_j| d^- d^- |\uparrow_i\uparrow_j\rangle \;=\; -\mu^2_{01}(w_i s_i^* v_j w_j^* + v_i w_i^* w_j s_j^*), \tag{S10}$$

where $d_0 = \langle 0,0|d^z|0,0\rangle$ and $\mu_{01} = \langle 1,\pm 1|d^\pm|1,0\rangle$ is the transition dipole moment between $|1,0\rangle$ and $|1,\pm 1\rangle$. From H_{dd} there also exists an on-site potential $t_{ii} = \sum_{j\neq i}(\langle\downarrow_i\downarrow_j| H_{dd} |\downarrow_i\downarrow_j\rangle - \langle\uparrow_i\downarrow_j| H_{dd} |\uparrow_i\downarrow_j\rangle)$ which varies between sites; however, as we will see below, inhomogeneities in t_{ii} can be regulated using optical lattice tensor shifts. Finally, we note that we have dropped a uniform chemical potential term associated with the molecule's rotational constant $2B$ (see Fig. 1B of the maintext).

To obtain topological flat bands, we adjust the optical radiation to generate four different types of sites $\{a, b, A, B\}$ (in relation to the M-scheme). By restricting the variation of $|\uparrow\rangle$ on (a vs. A) sites and on (b vs. B) sites, we ensure that both t_{ij} and V_{ij} are invariant under the direct lattice vectors $\vec{g}_1, \vec{g}_2$, enhancing the symmetry to that of a checkerboard lattice with a two-site

translational unit cell. This small generalization from a two-site model provides an important minus-sign freedom in the choice of w between lowercase and uppercase letter sites, which we exploit in tuning the Chern band structures. The freedom can be seen by examining the constraints imposed by requiring t_{ij} and V_{ij} to be invariant under $a \leftrightarrow A$ and $b \leftrightarrow B$ (*i.e.* translation by $\mathbf{g}_2$). In particular, the relevant constraints allow $w_{a/b} = w_{A/B}$ or $w_{a/b} = -w_{A/B}$ as solutions.

II. DETAILS FOR EXPERIMENTAL IMPLEMENTATION IN ^{40}K^{87}RB

1. *Hyperfine structure*

In this section, we consider the effects of the hyperfine structure of diatomic polar molecules such as ^{40}K^{87}Rb. The molecular rotational degree of freedom is naturally coupled to the nuclear spins, $I_1 = 4$ and $I_2 = 3/2$ of potassium and rubidium. The hyperfine Hamiltonian is dominated by the nuclear quadrupole interaction, which has a typical strength $H_Q \sim 1$MHz (for ^{40}K^{87}Rb). This interaction splits the degeneracy between the $|1, \pm 1\rangle$ rotational states implying that our workhorse, the $T^2_{\pm 2}$ terms of H_{dd}, are off-resonant. To overcome this issue, one can simply ensure that the optical dressing Ω (in the M-scheme) is much stronger than H_{hf}. This ensures that the hyperfine interaction is unable to couple the dark state to other dressed eigenstates.

We now consider the particular choice of nuclear spin states. Since the composition of the dark state differs on the four types of lattice sites $\{a, b, A, B\}$, molecules on these sites are subject to slightly different hyperfine potentials; in particular, $\langle\uparrow_A| H_{hf} |\uparrow_A\rangle = \langle\uparrow_a| H_{hf} |\uparrow_a\rangle \neq \langle\uparrow_B| H_{hf} |\uparrow_B\rangle = \langle\uparrow_b| H_{hf} |\uparrow_b\rangle$. Furthermore, the appropriate nuclear eigenstates will also depend on whether we are considering the rovibrational ground state ($|\downarrow\rangle$) or the dark state ($|\uparrow\rangle$); this is because the decoupled nuclear spin basis (so-called Paschen-Bach regime) is only valid in the first case. One can solve this issue by applying a static magnetic field $\sim 10^3$ G along the direction of the DC electric field. Then, it only remains to choose a pair of nuclear eigenstates (one for each of $|\uparrow\rangle$ and $|\downarrow\rangle$) which have reasonable overlap and resonant energies. We have numerically verified that this is generically achievable.

We now briefly discuss the effective conservation of particle number in our system. There are two processes that can cause a change in the spin-flip particle number. The ultimate limit is given by the lifetime of the molecules owing to off-resonant scattering from the 1064nm laser used to create the lattice. In the current generation of experiments, this lifetime can be extremely long (> 30s) and hence direct decay of the bare $J = 0, 1$ states can be safely neglected. This is similarly true for the dressed state ($|\uparrow\rangle$), since it is a dark state of the M-scheme and is composed solely of $J = 1$ states with no admixture of the two excited states. The second process originates from the off-resonant depolarization and dephasing of $|\uparrow\rangle$ via the dipolar and hyperfine interaction. For KRb, the dipolar interaction at 532nm is $\kappa \sim 1$kHz while the rotational splitting between the $J = 0$ and $J = 1$ states is $B \sim 1$GHz. Thus, the off-resonant dipolar-induced population in $J = 1$ is suppressed by $(\kappa/B)^2 \sim 10^{-12}$. When one turns on the optical dressing, the relevant splitting becomes the energy difference between dressed eigenstates which is of order the optical Rabi frequency $\Omega \sim 30$MHz. In this case, the suppression is $(\kappa/\Omega)^2 \sim 10^{-8}$. Finally, the dominant off-resonance error arises from hyperfine induced dephasing which couples the dark state to other dressed eigenstates. With a quadrupole dominated hyperfine interaction of $A \sim 1$MHz, similar estimates now lead to $(A/\Omega)^2 \sim 10^{-3}$.

2. *Tensor Light Shifts*

Similar to the hyperfine potential, A-type and B-type sites feel different tensor shifts from the optical lattice. As alluded to in the main text, these tensor shifts can be exploited to compensate for dipolar induced t_{ii} terms. To start, let us consider a single optical field, $E(R, t) = E(R)e^{-i\omega t} + \text{h.c.}$ which we use to create the lattice potential in the $\hat{X}$ direction. The optical potential is given by $H_{lattice} = -E(R)^* \alpha(\omega) E(R)$, where $E(R) = |E(R)| \sum_p \beta_p(R) e_p$, e_p is the polarization basis, and $\alpha(\omega)$ is the polarizability tensor of the molecule. Recasting the lattice potential in terms of spherical harmonics yields [27-29],

$$H_{lattice} = -E^2(R) \left[\frac{2\alpha_\perp - \alpha_\parallel}{3} + (\alpha_\parallel - \alpha_\perp) \sum_p C_p^2 \gamma_p \right] \tag{S11}$$

where $\alpha_\parallel$ is the polarizability along the internuclear axis, $\alpha_\perp$ is the polarizability transverse to the internuclear axis, $\gamma_0 = |\beta_0|^2 - 1/3$, $\gamma_{\pm 1} = 1/\sqrt{3}(\beta_0^* \beta_\pm - \beta_\mp^* \beta_0)$, and $\gamma_{\pm 2} = -\sqrt{2/3}\beta_\mp^* \beta_\pm$.

In our case, the optical lattice potential seen by $|\downarrow\rangle$ is,

$$\langle\downarrow| H_{lattice} |\downarrow\rangle = -E^2(R) \left[\frac{2\alpha_\perp - \alpha_\parallel}{3} + (\alpha_\parallel - \alpha_\perp) \langle 0, 0| C_0^2 |0, 0\rangle \gamma_0 \right] \tag{S12}$$

while the potential seen by $|\uparrow\rangle$ is,

$$\begin{aligned}\langle\uparrow|\, H_{lattice}\,|\uparrow\rangle &= -E^2(R)[\frac{2\alpha_\perp-\alpha_\parallel}{3}+(\alpha_\parallel-\alpha_\perp)\{\gamma_0(|s|^2\,\langle 1,-1|\,C_0^2\,|1,-1\rangle \\ &+ |v|^2\,\langle 1,1|\,C_0^2\,|1,1\rangle+|w|^2\,\langle 1,0|\,C_0^2\,|1,0\rangle)+\gamma_2 sv^*\,\langle 1,1|\,C_2^2\,|1,-1\rangle \\ &+ \gamma_{-2}s^*v\,\langle 1,-1|\,C_{-2}^2\,|1,1\rangle\}]. \end{aligned} \tag{S13}$$

The energy difference $\delta E = \langle\uparrow|\, H_{lattice}\,|\uparrow\rangle - \langle\downarrow|\, H_{lattice}\,|\downarrow\rangle$ varies between A-type and B-type sites since the dressing parameters $\{s, v, w\}$ are site-dependent. The goal is to use this tunable tensor shift to compensate for dipolar induced t_{ii} terms. Note that we can achieve propagation of the optical beams along any direction using only σ_+ and π light. Since our optical field never contains any σ_- polarization, we find that $\gamma_{\pm 2}$ terms are zero. Moreover, we have also dropped $\gamma_{\pm 1}$ terms, since $\Delta = E_{1,0} - E_{1,1} \gg H_{lattice}$. Combining the optical fields propagating along the $\hat{x}$, $\hat{y}$ and $\hat{z}$ direction (to create the 3D lattice), we have numerically verified that by simply adjusting the intensities of the lattice light, we can fully compensate for any inhomogeneous on-site potential.

Finally, we demonstrate a simple configuration of Raman lasers (with wavelength λ_0), which generates the M-scheme for the $\{a, b, A, B\}$ checkerboard lattice shown in Fig. 2A. We take the lattice constant to be $\lambda_L = R_0$ (Fig. 2A) and assume that $\lambda_0 \leq \lambda_L$; this can always be accomplished by increasing λ_L (at the expense of weaker dipolar interactions). We can tilt the k-vectors propagating along $\hat{X}$ and along $\hat{Y}$ up or down out of the XY plane to give them a periodicity of λ_L (in the XY plane). We can also tilt the k-vectors propagating along $(\hat{X} \pm \hat{Y})$ up or down out to give them a periodicity of $\sqrt{2}\lambda_L$ (in the XY plane). By using only four out of these eight beams and linearly polarizing them along $\hat{k} \times \hat{z}$, we can obtain arbitrary Ω_2 and Ω_3 on A and B sites with $\Omega_1 = \Omega_4 = 0$. Similarly, we can obtain arbitrary $\Omega_1 = \Omega_4$ on A and B sites (and their negatives on a and b sites) with $\Omega_2 = \Omega_3 = 0$. This immediately enables us to construct the four-site M-scheme.

3. Dipolar Temperature Scales

The current generation of polar molecule experiments harbor dipole moments of: RbCs [1.2D], NaK [2.8D], KRb [0.6D], LiCs [5.5D], [LiK 3.6D]. At 532nm lattice spacing, the typical dipolar interaction between two molecules with a ~ 3 Debye dipole moment is $\sim$ 20kHz corresponding to a temperature $T \sim 1\mu$K. The current RbCs and KRb experiments have both realized ground state molecules cooled to temperatures $\sim$ 100nK. Along similar lines, fermionic NaK feshbach molecules have also recently been generated. Moreover, in our current proposal, it is sufficient for the motional temperature to be below the bandgap energy, which is approximately 100kHz. The "spin temperature" is much lower than the motional temperature and, before the optical dressing is turned on, is simply a function of how well one can prepare the rovibrational ground state. As a final point worth mentioning, it may be possible to work at significantly smaller optical lattice spacings 340nm (KRb) and 395nm (RbCs). Since the dipolar interaction scales as $1/r^3$, this can even further increase the dipolar energetics and hence the gap scales.

III. DERIVATION OF MANY-BODY PHASES

Here, we provide a detailed description of the many-body phases which arise as one tunes the electric field parameters. First, we note that the field and dressing parameters for the phase diagram (Fig. 1C) are different than those for Figures 2B and 3. This is because the richest many-body phase diagram that we observe does not occur for the band structure with the largest flatness ratio. The band-structure depicted in Fig. 2B occurs at electric field tilt $\Theta_0 = 0.68, \Phi_0 = 5.83$, with optical dressing parameters: $\{\theta_a, \theta_b, \phi_a, \phi_b, \alpha_a, \alpha_b, \gamma_a, \gamma_b\} = \{0.53, 0.97, 1.36, 3.49, 2.84, 2.03, 4.26, 3.84\}$, where we have parametrized: $s_i = \sin(\alpha_i)\sin(\theta_i)$, $v_i = \sin(\alpha_i)\cos(\theta_i)e^{i\phi_i}$ and $w_i = \cos(\alpha_i)e^{i\gamma_i}$.

The phase diagram shown in Fig. 1C is computed by exact diagonalization for filling fraction $\nu = 1/2$ and a total of $N_s = 24$ sites (parameters: $\{\Theta_0, \Phi_0, \theta_a, \theta_b, \phi_a, \phi_b, \alpha_a, \alpha_b, \gamma_a, \gamma_b\} = \{0.65, 3.68, 2.4, 2.97, 6.06, 4.1, 0.97, 2.74, 3.44, 1.74\}$). The associated band-structure has a flatness ratio, $f \approx 7$. The dressing parameters on A-type and B-type sites are identical to those on a and b sites with the exception that $\gamma_A = \pi + \gamma_a$ and $\gamma_B = \pi + \gamma_b$ (*ie.* $w_{a/b} = -w_{A/B}$). At weak electric fields, $E \lesssim 8$ kV/cm, diagonalization reveals the $\nu = 1/2$ Fractional Chern Insulator. By changing both the strength and tilt (Θ_0) of the DC field, one can map out a phase diagram containing both conventional and topological phases. To isolate the effects of long-range interactions, we ensure that at each tilt, the flatness ratio remains the same for all DC field strengths. This can be achieved by re-optimizing the dressing parameters for each field strength. Alternatively, this corresponds to ensuring that $d_{00} = d_{01}$ as the field increases; experimentally, one can realize this by dressing the $|1, \pm 1\rangle$ states with a long-lived metastable excited state. Numerically, we implement this constraint by taking $s_i \to s_i d_{00}/d_{01}$ and $v_i \to v_i d_{00}/d_{01}$.

There exist four crystalline phases at strong DC electric fields whose diagnostics we depict in Fig. S1. At low and intermediate DC field strengths, we observe a large superfluid region. This phase is characterized by a unique ground state (typically in either

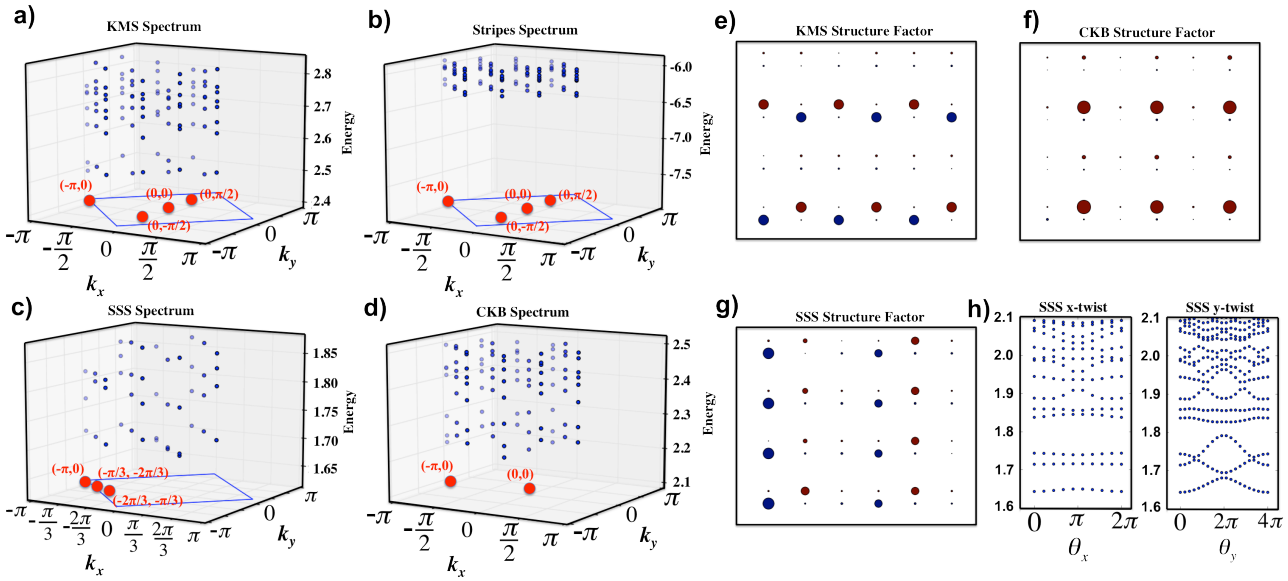

FIG. S1: — Many-body Phases. (a) Depicts the spectrum associated with the knight's move solid phase in the reduced Brillouin zone (k_x and k_y are crystal momenta). The electric field tilt is $\Theta_0 = 0.05$ and the field strength is $|E| \sim 32$kV/cm. (b) depicts the spectrum associated with the striped phase ($\Theta_0 = 1.05$ and $|E| \sim 28$kV/cm). (c) depicts the spectrum associated with the striped supersolid phase ($\Theta_0 = 0.68$ and $|E| \sim 36$kV/cm). (d) depicts the spectrum associated with the checkerboard phase ($\Theta_0 = 0.25$ and $|E| \sim 40$kV/cm). (e-g) depicts the structure factor of the KMS, CKB, SSS respectively for the same parameters as above (SS phase omitted). (h) depicts the spectral flow under magnetic flux insertion of the SSS phase. $\hat{X}$-boundary condition twists produce little dispersion in the ground state energy while $\hat{Y}$ twists yield markedly superfluid behavior. Boundary conditions twists in both $\hat{X}$ and $\hat{Y}$ directions yield minimal superfluid response for the KMS, CKB and SS phases (not shown).

the $(0, 0)$ or $(-\pi, 0)$ momentum sectors) and a fluid-like real space structure factor. The homogeneity of the superfluid changes as one adjusts the DC field strength and tilt. At very weak fields $|E| < 4$kV/cm, A-type and B-type sites are equally populated; however, as one increases the field strength, the anisotropy of the long-range dipolar interaction yields anisotropy in the structure factor.